

A WIDEBAND DUAL-POLARIZED PATCH ANTENNA WITH ELECTRIC PROBE AND MAGNETIC LOOP FEEDS

J.-J. Xie^{*}, Y.-Z. Yin, J. Ren, and T. Wang

National Laboratory of Antennas and Microwave Technology, Xidian University, Xi'an, Shaanxi 710071, China

Abstract—A new wideband dual-polarized patch antenna consisting of a magnetically-fed and an electrically-fed is presented in the paper. The two feeds are orthogonal to each other at the center of the ground plane and generate 0° and 90° polarization separately. Two pairs of L-shaped slots are etched in the radiating patch to improve the impedance bandwidth. By using a shorting pin connecting the radiating patch to the ground plane, the coupling between the two feeding ports can be reduced. With the help of circuit simulation and full wave simulation, the equivalent circuit model of the antenna is established. The simulated and measured results show that the impedance bandwidths for VSWR less than 2 of the proposed dual-polarized antenna with a profile of are 27.3% (3.29–4.33 GHz) and 19% (3.05–3.69 GHz) for 0° polarization and 90° polarization, respectively, with a height of $0.08\lambda_0$ between radiating patch and ground plane. The measured coupling between the two ports is below -20 dB over the operating band. Moreover, the maximum gain of the proposed antenna is about 8.5 dBi and 6.9 dBi for port 1 and port 2, respectively, over the operating band. Measured results of the fabricated antenna prototypes are in good agreement with the simulated results.

1. INTRODUCTION

With the rapid progress of wireless communications, the capacity issue is becoming critical due to the expansion of wireless services and the increasing of mobile subscribers. Research work has been focused on frequency reuse and polarization diversity by using two orthogonal polarizations [1–3]. Antennas with polarization diversity

Received 31 August 2012, Accepted 9 October 2012, Scheduled 11 October 2012

* Corresponding author: Jiao-Jiao Xie (xiejiaojiaocye@gmail.com).

performance are widely studied and adopted to mitigate the multipath-fading problem in WiMAX application. Moreover, they are able to provide double transmission channels and increase channel capacity per frequency in many applications [4, 5]. Therefore, dual polarization antennas with wide bandwidth, compact size and low cost are highly desirable for modern wireless communication applications.

To fulfill the increasing demand of channel capacity, several types of dual-polarized antennas have been designed and studied in recent papers, including microstrip patch antennas with probe feed [6–8], stacked microstrip antennas with aperture coupling [9, 10], and horn antennas [11–13]. Two coaxial lines were used in [6] to excite the radiating patches and produce dual polarization performance. Although the antenna had a high isolation, it was large in size. The dual-polarized planar antenna was excited by the probe in [7]. However, the average bandwidth of the dual polarization was only 8%. A dual-band dual-mode dual-polarization antenna was excited by four pins in [8]. By using a composite right/left handed transmission line in the feed line, the phase of the feed network can be controlled easily. However, the impedance bandwidth was only 3.8% for the conical mode. A crossed coupling slot was used to feed the antenna in [9] for achieving dual polarization radiation, but the size of the proposed antenna was too large. Two vertically stacked multilayered Yagi antennas with single and dual polarizations were presented in [10], the high gain was obtained by increasing the number of the layers. However, the antennas had a complicated structure and large size. A dual-polarized horn antenna excited by a gap-fed square patch was proposed in [11]. However, it was narrow in bandwidth. A double-ridged horn antenna with wide bandwidth was presented in [12]. However, it required five layers polarizer to provide dual polarization performance, which increased the complexity of the antenna. A dual-polarized dielectric-loaded horn antenna fed by pairs of balanced coaxial cables was designed in [13] for ultra-wideband applications. Microwave absorbers and conductive enclosure were employed to stabilize the radiation patterns, but the antenna was high in cost.

Due to its various advantages including low profile, light weight, and easy fabrication for dual polarization implementation, the patch antenna has been widely studied and employed [14–18]. However, the patch antenna is narrow in bandwidth [14, 15]. Several methods have been proposed to improve the impedance bandwidth of the patch antenna. With the use of electromagnetic bandgap superstrates, the impedance bandwidth of a probe-fed microstrip antenna was enhanced [19]. A thick wedge-shaped air substrate was used for probe-fed patch antenna to reduce the size of the radiating patch and broaden

the impedance bandwidth [20]. A crescent like shaped patch was used for the single-layer probe-fed microstrip patch antenna to improve the impedance bandwidth [21]. Recently, a loop-fed technology consisted of a metal loop and an open-ended transmission line was introduced to enhance the bandwidth of the patch antenna [22]. Stable and regular radiation patterns were demonstrated.

In this paper, a new design of a dual-polarized patch antenna with a wide impedance bandwidth is presented, built and tested for WiMAX application. The proposed antenna consists of a magnetically-fed patch antenna element and an electrically-fed patch antenna element, which are orthogonal to each other at the center of a ground plane. To suppress the coupling between the two feeding ports, a shorting pin is used to connect the radiating patch to the ground plane. Two equivalent circuit models of the linearly polarization elements are developed for the ease of design. The dual resonance performance of the linearly polarization antennas can be demonstrated in detail by these circuit models. Two linearly polarization antennas are described first to explain the principle of operation. With the help of the proposed two equivalent circuit models, a new circuit model of the wideband dual-polarized antenna is designed. The equivalent circuit model assists in the initial design, and then minor modifications are required to achieve the desired dual polarization performance. Finally, the proposed antennas are fabricated and measured to validate the design method.

2. LINEARLY POLARIZED WIDEBAND ANTENNA

2.1. Electrically-fed Patch Antenna (Antenna #1)

2.1.1. Antenna Design

The top and side views of the electrically-fed patch antenna are shown in Fig. 1. The radiating patch is printed on a 1-mm-thick FR4 substrate with the dielectric constant (ϵ_r) of 4.6 and the loss tangent ($\tan \delta$) of 0.02. The distance between the dielectric substrate and the ground plane is $0.13\lambda_0$, where λ_0 is the free space wavelength at the center frequency. The antenna is fed by a coaxial pin that is placed along the x -axis of the radiating patch and located at a distance of D from the boundary of the patch. A shorting pin is also placed along the x -axis and symmetrical with the feeding pin. To reduce the effect of the inductive reactance associated with the long probe pin in the thick air and achieve good impedance matching over a wide operating bandwidth, two pairs of L-shaped slots with the same length and width are inserted at the edge of the radiating patch. The desired

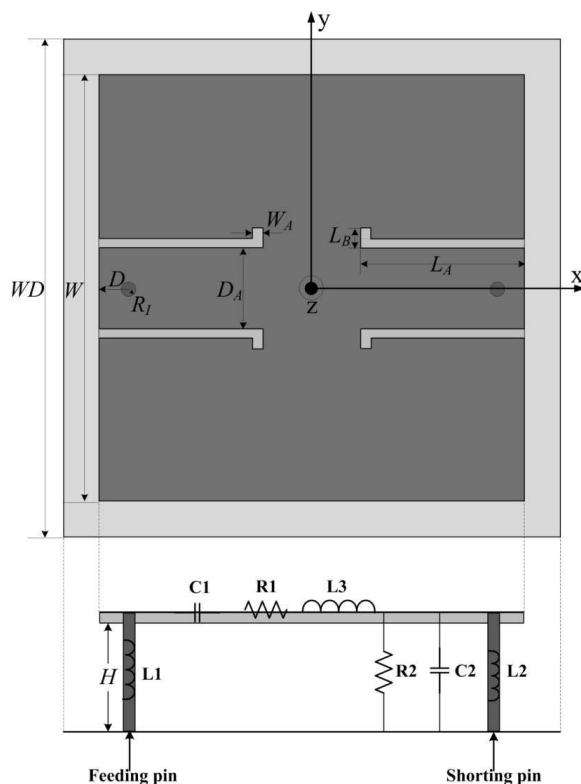


Figure 1. Geometry of antenna #1. ($WD = 50$ mm, $W = 43$ mm, $H = 11$ mm, $L_A = 16.5$ mm, $L_B = 2$ mm, $W_A = 1$ mm, $D_A = 8$ mm, $D = 3$ mm, $R_I = 0.6$ mm).

wideband operation of the proposed antenna can be realized by the proper placement of the shoring pin and the L-shaped slits.

2.1.2. Equivalent Circuit

The equivalent circuit model superimposed over the side view of the electrically-fed patch antenna is also depicted in Fig. 1. This circuit model which composed of a series resonant circuit and a parallel resonant circuit helps the analysis of the dual resonance performance of the antenna [23]. The radiating patch acting as an inductor (L_3) has a capacitive coupling (C_2) to the metal ground plane [24]. The resistance (R_1) in the radiating patch represents the sum of the radiation reactance, dielectric loss and surface wave loss [25]. A coaxial

probe acting as an inductor (L_1) is used to excite the antenna and generate a single resonant mode as shown in Fig. 2. A shorting pin playing as a shunt inductor (L_2) connects the radiating patch to the ground plane and forms a parallel resonant circuit, which makes the resonant frequency shift to higher. However, a bad impedance matching is caused by the large probe reactance (R_2) owing to the long probe pin in the thick air substrate. By etching two pairs of L-shaped slots in the radiating patch in the vicinity of the feeding pin and shorting pin, a capacitor (C_1) is added in the radiating patch which forms a new series resonant circuit and compensates the large probe reactance. In this case, two adjacent resonant modes for the proposed antenna can be excited with good impedance matching, and a wide impedance bandwidth is obtained by the two adjacent resonant modes.

To examine whether the equivalent circuit model can predict the dual resonance performance of the proposed electrically-fed patch antenna, the values of the lumped elements in Fig. 3(a) are first derived from the design parameters in Fig. 1 and slightly adjusted, based on full wave simulation results. Fig. 3(b) shows the real and imaginary parts of input impedance which are derived from a circuit (Advanced Design System 2008) and full wave (Ansoft HFSS 12) simulators. The circuit and full wave simulated S parameter results of the antenna are depicted in Fig. 4. It is seen that the two results are in very good agreement, meaning that the equivalent circuit model can predict the performance perfectly.

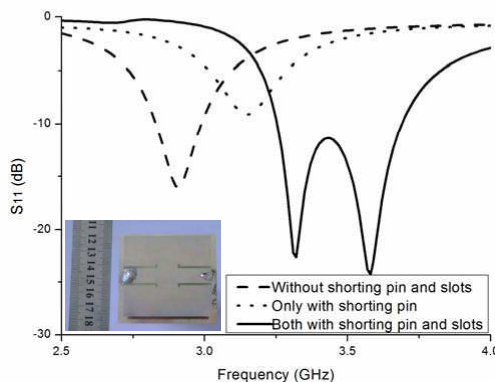


Figure 2. Simulated S_{11} of antenna #1 without/with shorting pin or slots.

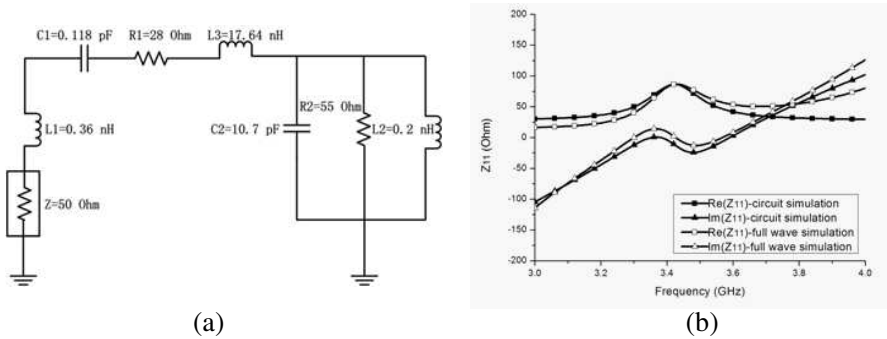


Figure 3. (a) Equivalent circuit model of antenna #1; (b) Real and imaginary parts of input impedance simulated by circuit and full wave simulators.

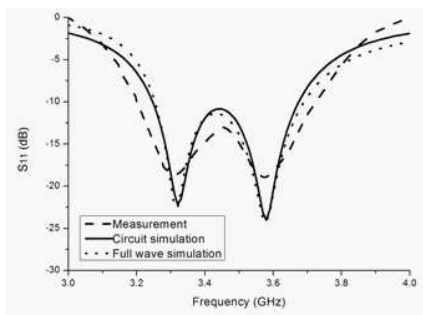


Figure 4. Measured, circuit and full wave simulated S_{11} of the antenna #1.

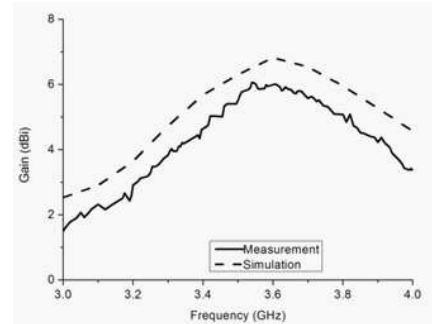


Figure 5. Measured and simulated gain of the antenna #1.

2.1.3. Simulation and Measurement Results

The fabricated prototype of the proposed electrically-fed patch antenna is measured by a WILTRON37269A vector network analyzer and a fully automated anechoic chamber. The measured S parameter result is also given in Fig. 4. The simulated impedance bandwidth is 12.7% from 3.25 GHz to 3.69 GHz, while the measured impedance bandwidth is 15% from 3.21 GHz to 3.73 GHz. The measured impedance bandwidth is slightly wider than the simulated result. This may be due to the effect of connector losses. The simulated and measured gain are depicted in Fig. 5. The simulated gain of the antenna is about 6 dBi over the operating band from 3.25 GHz to 3.69 GHz, while the measured gain is about 5 dBi over the operating band from 3.21 GHz

to 3.73 GHz. The 1 dB drop in measured gain may be caused by the imperfections of the compact range anechoic chamber used and also by losses such as surface waves, dielectric losses, and little ground plane. The measured radiation patterns at 3.3 GHz and 3.6 GHz are plotted in Fig. 6. As shown in the figures, the levels of cross polarization are generally less than -10 dB.

2.2. Magnetically-fed Patch Antenna (Antenna #2)

2.2.1. Antenna Design

The configuration of the magnetically-fed patch antenna is shown in Fig. 7. The proposed antenna is a combination of a microstrip patch antenna, which is horizontally oriented, and a magnetically-coupled loop antenna, which is vertically oriented. The microstrip patch is printed on a 1-mm-thick horizontal FR4 substrate with a height of $0.19\lambda_0$, where λ_0 is the free space wavelength at the center frequency. The horizontal substrate is supported by plastic posts. The metal loop with a gap $G = 1$ mm is printed on one side of the 1-mm-thick vertical FR4 substrate with the dielectric constant (ϵ_r) of 4.6 and the loss tangent ($\tan \delta$) of 0.02. The antenna is excited magnetically through an open-ended microstrip transmission line of the loop printed on the other side of the vertical dielectric substrate. The open-ended strip with a tunable length L_s is used to resonant with the metal loop and couple magnetically to the top patch antenna simultaneously.

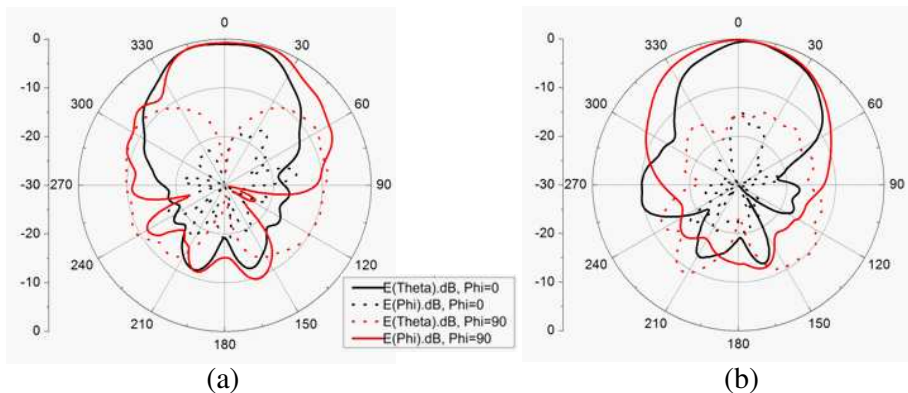


Figure 6. Measured radiation patterns at (a) 3.3 GHz and (b) 3.6 GHz.

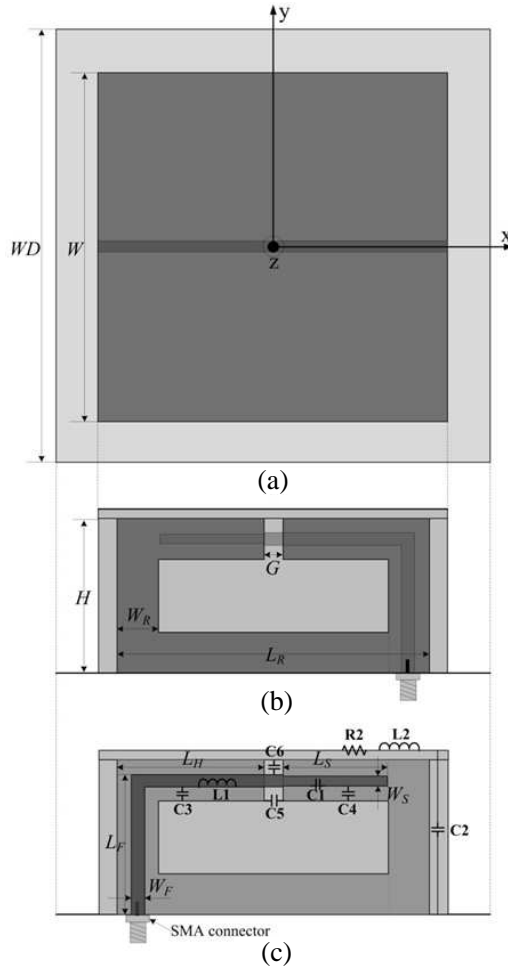


Figure 7. Configuration of antenna #2. (a) Top view; (b) Side view (from $+y$ -axis); (c) Side view (from $-y$ -axis) ($WD = 50$ mm, $W = 40$ mm, $H = 18$ mm, $L_R = 36$ mm, $W_R = 5$ mm, $G = 1$ mm, $L_F = 16.25$ mm, $W_F = 1.5$ mm, $L_H = 16.75$ mm, $L_S = 12.5$ mm, $W_S = 1.3$ mm).

2.2.2. Equivalent Circuit

The equivalent circuit model of the proposed magnetically-fed patch antenna is also given in Fig. 7(c). It consists of a parallel resonant circuit and a series resonant circuit. The microstrip patch acting as an inductor (L_2) has a capacitive coupling (C_2) to the metal ground plane.

The resistance (R2) in the horizontal microstrip patch represents the sum of the radiation reactance, dielectric loss and surface wave loss. The microstrip transmission line playing as an inductor (L1) has a capacitive coupling (C3) to the metal loop. The open-ended strip which also has a capacitive coupling (C4) to the loop, is used as a capacitor (C1) to resonant with the microstrip transmission line and generate a magnetic coupling (C6) to excite the top patch. Additional capacitance (C5) is introduced due to the gap in the loop.

In order to resonant near the frequency of the patch antenna and broaden the impedance bandwidth, the length L_s of the open-ended strip is approximately given by

$$L_s \approx \frac{\lambda_{01}}{4} \cdot \frac{1}{\sqrt{\epsilon_r}} \tag{1}$$

where ϵ_r is the relative dielectric constant of the substrate and λ_{01} the free space wavelength of the first resonant mode. To corroborate the rationality of the expression, Fig. 8 shows the S_{11} of the proposed loop feed patch antenna for different values of L_s . It is seen that two close resonant modes are excited and a wideband impedance bandwidth can be obtained when the open-ended strip length L_s is about $0.25\lambda_1$.

The values of the lumped elements in Fig. 9(a) are derived from the circuit simulator. To check the validity of the equivalent circuit model, the real and imaginary parts of input impedance which are derived from a circuit and full wave simulators are shown in Fig. 9(b). The circuit and full wave simulated S_{11} of the proposed magnetically-coupled loop antenna are shown in Fig. 10. Good agreement between the two results is achieved, meaning that the equivalent circuit model is reasonable.

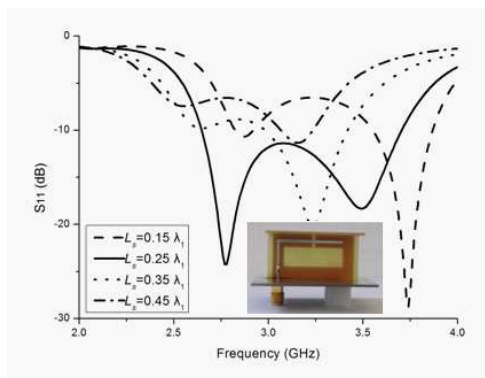


Figure 8. Simulated S_{11} of antenna #2 for different values of L_s .

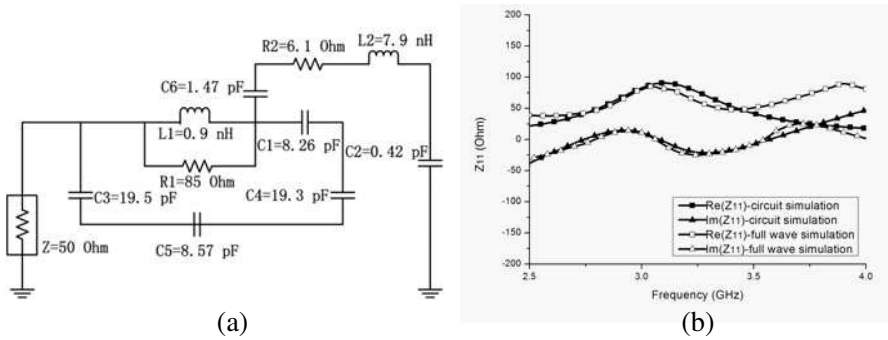


Figure 9. (a) Equivalent circuit model of antenna #2; (b) Real and imaginary parts of input impedance simulated by circuit and full wave simulators.

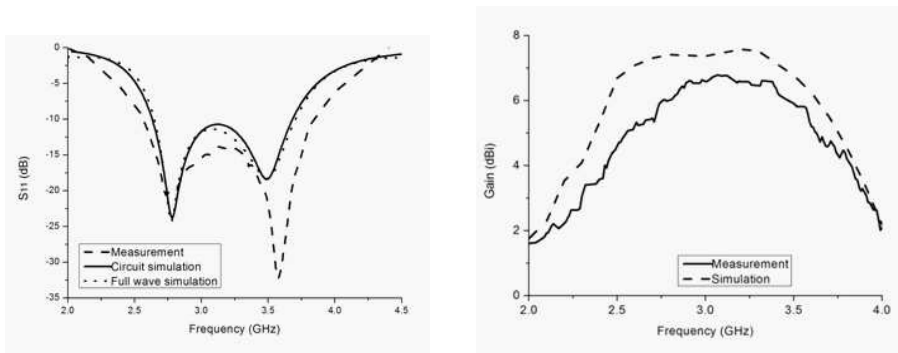


Figure 10. Measured, circuit and full wave of simulated S_{11} of the antenna #2.

Figure 11. Measured and simulated gain the antenna #2.

2.2.3. Simulation and Measurement Results

The simulated and measured S_{11} are presented in Fig. 10. From the results, it is seen that two adjacent resonant modes are excited, which leads to a wide bandwidth. The simulated impedance bandwidth is 33.3% from 2.65 GHz to 3.71 GHz, and the measured impedance bandwidth is 39% from 2.56 GHz to 3.84 GHz.

The slight difference between simulated and measured results is mainly contributed from material losses. The simulated gain of antenna shown in Fig. 11 is about 6.8 dBi over the operating band from 2.65 GHz to 3.71 GHz while the measured gain is about 6.2 dBi over the operating band from 2.56 GHz to 3.84 GHz. A mild gain drop in the measurement is caused by the small ground plane. The measured

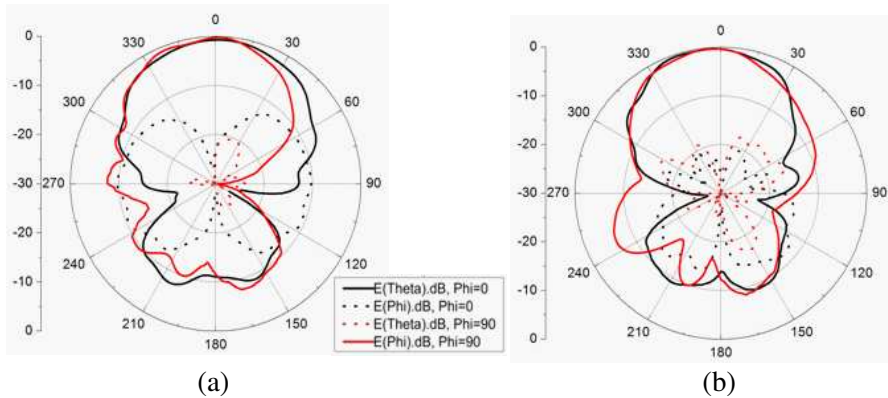


Figure 12. Measured radiation patterns at (a) 2.8 GHz and (b) 3.5 GHz.

radiation patterns of the antenna at 2.8 GHz and 3.5 GHz are given in Fig. 12. The levels of cross polarization depicted in the figure are generally less than 10 dB.

3. DUAL POLARIZED DUAL RESONANCE ANTENNA (ANTENNA #3)

3.1. Antenna Design

Based on the previous proposed linearly polarized antenna structures, a dual-polarized wideband antenna is designed and constructed by integrating an electrically-fed patch antenna and a magnetically-fed patch antenna with orthogonal orientation. The geometry of the dual-polarized wideband antenna is shown in Fig. 13. The radiating patch with four identical L-shaped slots is printed on the horizontal FR4 substrate with thickness of 1 mm and $\epsilon_r = 4.6$ for ease of construction and support. The L-shaped slots are placed symmetrical with the center of the patch. The height of the air substrate is $0.08\lambda_0$ at 3.5 GHz. The metal loop with a gap and an open-ended transmission line are printed on the vertical FR4 substrate. With the use of a shorting pin connected the radiating patch to the ground plane, the isolation between the two feeding ports is improved. Two SMA connectors located under the ground plane are connected to the ends of the coaxial probe and the transmission line of the metal loop, respectively. The antenna radiates 0° and 90° linearly polarized waves. When Port 1 is excited and Port 2 is connected to a match load, the antenna is 0° polarization (similarly Port 2 excites 90° polarized wave).

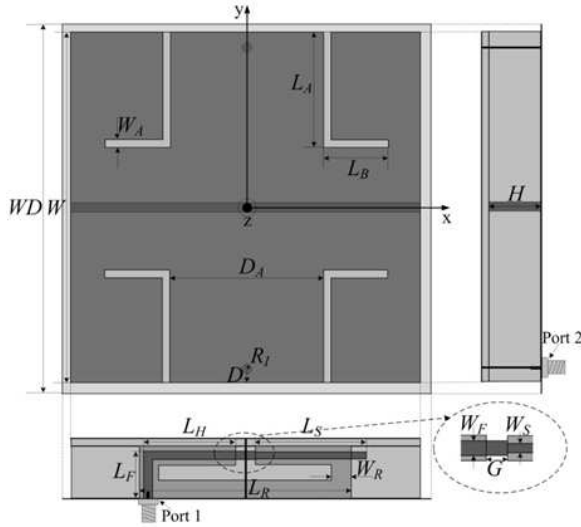


Figure 13. Geometry of the proposed antenna #3. ($WD = 48$ mm, $W = 46$ mm, $H = 7$ mm, $L_A = 15$ mm, $L_B = 8.5$ mm, $W_A = 1$ mm, $D_A = 20$ mm, $D = 2$ mm, $R_I = 0.6$ mm, $L_R = 28$ mm, $W_R = 2.5$ mm, $G = 2.5$ mm, $L_F = 6.35$ mm, $W_F = 1.2$ mm, $L_H = 14.6$ mm, $L_S = 14.6$ mm, $W_S = 1$ mm).

3.2. Equivalent Circuit

Based on the previous analysis, the proposed electrically-fed patch antenna is equivalent to a series resonant circuit and a parallel resonant circuit, and the proposed magnetically-fed patch antenna can be equivalent to a parallel resonant circuit and a series resonant circuit. Thus, the equivalent circuit of the antenna #3 can be seen as a combination of these resonant circuits. As depicted in Fig. 14(a), the two feeding structures acting as a transformer are inductively coupled. The coupling coefficient (L_{12}) of the transformer corresponds to the distance between the microstrip transmission line and the coaxial probe. The capacitor (C_{12}) is introduced due to the common radiating patch of the magnetically-fed patch antenna and electrically-fed patch antenna. Finally, the equivalent circuit model of the proposed wideband dual-polarized antenna can be obtained by the curve fitting method. The circuit and full wave simulated S parameters of the proposed dual-polarized antenna are shown in Fig. 14(b). It is found that the results agree well, which means that the equivalent circuit model is rational.

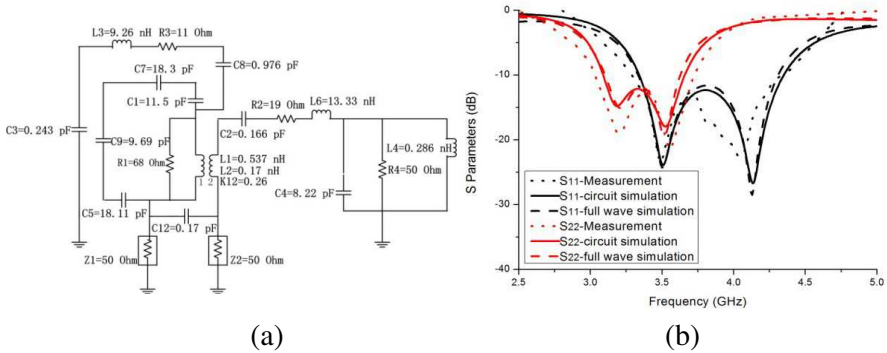


Figure 14. (a) Equivalent circuit model of the proposed antenna #3; (b) Measured, circuit and full wave simulated S parameters of the proposed antenna #3.

3.3. Simulation and Measurement Results

The measured S parameters of the proposed antenna are also depicts in Fig. 14(b). It is observed that, the measured impedance bandwidth is 27.3% (3.29–4.33 GHz) and 19% (3.05–3.69 GHz) at port 1 and port 2 respectively, while the simulated impedance bandwidth is 25.4% (3.34–4.31 GHz) and 16.1% (3.11–3.63 GHz) respectively. Good agreement between simulation and measurement of impedance bandwidth can be observed. A small difference between the measured and simulated results can be attributed to the fabrication accuracy. The measured and simulated isolation of the proposed antenna is plotted in Fig. 15. It is found that the isolation between the two feeding ports can be enhanced to more than 20 dB over the operating band by using the shorting pin.

The simulated and measured antenna gain over the operating band is illustrated in Fig. 16. It can be found that the maximum gain is about 8.5 dBi and 6.9 dBi for 0° polarization and 90° polarization, respectively, in the whole operating band. There is a little difference between the simulated and measured results, which may be caused by the non-ideal connector of the fabricated antenna. The measured radiation patterns of proposed dual-polarized antenna at port 1 and port 2 are plotted in Fig. 17. It can be observed that, the radiation pattern in broadside direction varies slightly with frequency at both ports. The main beam of the radiation is always fixed in the broadside z -direction.

The performance of the proposed antenna is compared with those of other dual-polarized antennas in Table 1. The comparison includes

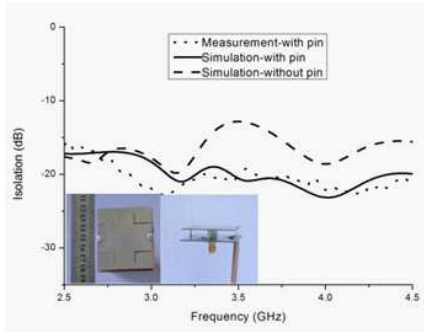


Figure 15. Isolation of the dual-polarized antenna with/without shorting pin.

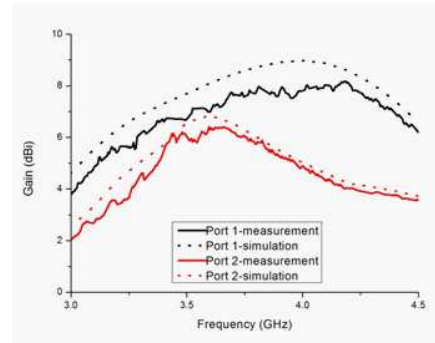


Figure 16. Gain of the dual-polarized antenna.

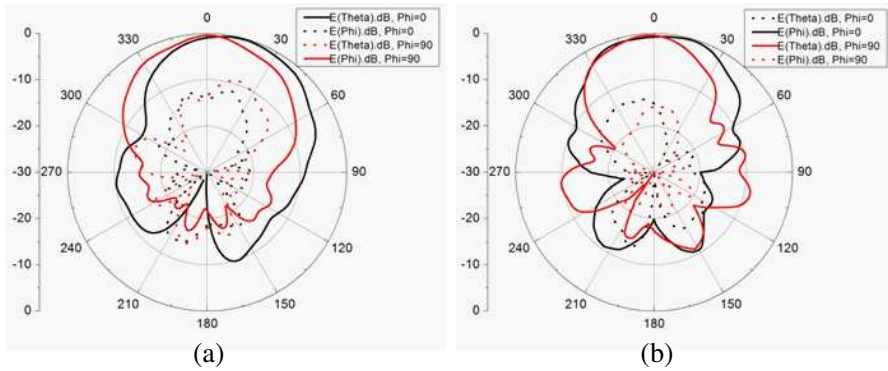


Figure 17. Measured radiation patterns of the antenna #3 at 3.5 GHz. (a) port 1, and (b) port 2.

Table 1. Comparison of the dual-polarized antennas.

Antenna type	Height (mm)	BW (%)	Isolation (dB)	Maximum gain (dBi)
Planar antenna	$0.3\lambda_0$	8	-20	12.8
Stack antenna	$1.16\lambda_0$	4	-25	9.76
Horn antenna	$1.1\lambda_0$	4	-30	12.34
Proposed antenna	$0.08 \lambda_0$	11	-20	8.5

the height, bandwidth, isolation, and gain of the proposed antenna against the microstrip patch antenna [7], the stacked microstrip antenna [10], and the horn antenna [11]. It can be seen that, the dual-polarized planar antenna with probe feed has the improved gain due to the bigger array size in the horizontal plane. Both the stacked microstrip antenna and horn antenna have a narrow bandwidth and high profile. For the proposed antenna, the impedance bandwidth is improved due to the dual resonance performance. Moreover, the new antenna has a lower profile than other dual-polarized antenna.

4. CONCLUSION

A new wideband dual-polarized patch antenna with electromagnetic feeding structure is proposed in this paper. The 0° polarization is provided by the magnetically-coupled loop antenna, and the 90° polarization is provided by the electrically-fed patch antenna. Good isolation is obtained by the shorting pin connecting the radiating patch to the ground plane. Two linearly polarization antenna configurations are first presented and studied. With the help of circuit simulation and full wave simulation, the equivalent circuit models of the two linearly polarization elements are developed. The operation principle of the dual resonance performance can be demonstrated in detail by these circuit models. Based on the proposed two equivalent circuit models, a new circuit model of the dual-polarized antenna is designed. Finally, the proposed antennas are fabricated and tested. The measurement results are similar to the simulated results. Due to the wide impedance bandwidth and low profile, the proposed dual-polarized antenna shows the potential use for the WiMAX system.

REFERENCES

1. Peng, H.-L., W.-Y. Yin, J.-F. Mao, D. Huo, X. Hang, and L. Zhou, "A compact dual-polarized broadband antenna with hybrid beam-forming capabilities," *Progress In Electromagnetic Research*, Vol. 118, 253–271, 2011.
2. Soltani, S., M.-N. Azarmanesh, E. Valikhanloo, and P. Lotfi, "Design of a simple single-feed dual-orthogonal-linearly-polarized slot antenna for concurrent 3.5 GHz WIMAX and 5 GHz WLAN access point," *Journal of Electromagnetic Waves and Applications*, Vol. 24, No. 13, 1741–1750, 2010.
3. Secmen, M. and A. Hizal, "A dual-polarized wide-band patch antenna for indoor mobile communication applications," *Progress In Electromagnetic Research*, Vol. 100, 189–200, 2010.

4. Expósito-Domínguez, G., J.-M. Fernández-González, P. Padilla de la Torre, and M. Sierra-Castañer, "Dual circular polarized steering antenna for satellite communications in X band," *Progress In Electromagnetic Research*, Vol. 122, 61–76, 2012.
5. Wu, G.-L., W. Mu, G. Zhao, and Y.-C. Jiao, "A novel design of dual circularly polarized antenna FED by L-strip," *Progress In Electromagnetic Research*, Vol. 79, 39–46, 2008.
6. Liu, C., J.-L. Guo, Y.-H. Huang, and L.-Y. Zhou, "A novel dual-polarized antenna with high isolation and low cross polarization for wireless communication," *Progress In Electromagnetics Research Letters*, Vol. 32, 129–136, 2012.
7. Masa-Campos, J.-L. and F. González-Fernández, "Dual linear/circular polarized planar antenna with low profile double-layer polarizer of 45° tilted metallic strips for WiMAX applications," *Progress In Electromagnetic Research*, Vol. 98, 221–231, 2009.
8. Cao, W.-Q., B. Zhang, A. Liu, T. Yu, D. Guo, and Y. Wei, "Novel phase-shifting characteristic of CRLH TL and its application in the design of dual-band dual-mode dual-polarization antenna," *Progress In Electromagnetic Research*, Vol. 131, 375–390, 2012.
9. Moradi, K. and S. Nikmehr, "A dual-band dual-polarized microstrip array antenna for base stations," *Progress In Electromagnetic Research*, Vol. 123, 527–541, 2012.
10. Kramer, O., T. Djerafi, and K. Wu, "Vertically multilayer-stacked Yagi antenna with single and dual polarizations," *IEEE Trans. Antennas Propag.*, Vol. 58, No. 4, 1022–1030, Apr. 2010.
11. Ononchimeg, S., G. Otgonbaatar, J.-H. Bang, B.-C. Ahn, and E.-J. Cha, "A new dual-polarized horn antenna excited by a gapped square patch," *Progress In Electromagnetics Research Letters*, Vol. 21, 129–137, 2011.
12. Mallahzadeh, A.-R., A.-A. Dastranj, and H.-R. Hassani, "A novel dual-polarized double-ridged horn antenna for wideband applications," *Progress In Electromagnetics Research B*, Vol. 1, 67–80, 2008.
13. Chung, J.-Y., "Ultra-wideband dielectric-loaded horn antenna with dual-linear polarization capability," *Progress In Electromagnetics Research*, Vol. 102, 397–411, 2010.
14. Monavar, F. M. and N. Komjani, "Bandwidth enhancement of microstrip patch antenna using Jerusalem cross-shaped frequency selective surfaces by invasive weed optimization approach," *Progress In Electromagnetics Research*, Vol. 121, 103–120, 2011.
15. Montero-de-Paz, J., E. Ugarte-Muñoz, F. J. Herraiz-Martínez,

- V. González-Posadas, L. E. García-Muñoz, and D. Segovia-Vargas, "Multifrequency self-diplexed single patch antennas loaded with split ring resonators," *Progress In Electromagnetics Research*, Vol. 113, 47–66, 2011.
16. Xiong, J., H. Li, B.-Z. Wang, Y. Jin, and S. He, "Theoretical investigation of rectangular patch antenna miniaturization based on the DPS-ENG bi-layer super-slow TM wave," *Progress In Electromagnetics Research*, Vol. 118, 379–396, 2011.
 17. Zhu, X., W. Shao, J.-L. Li, and Y.-L. Dong, "Design and optimization of low RCS patch antennas based on a genetic algorithm," *Progress In Electromagnetics Research*, Vol. 122, 327–339, 2012.
 18. Alam, M. S., M. T. Islam, and N. Misran, "A novel compact split ring slotted electromagnetic bandgap structure for microstrip patch antenna performance enhancement," *Progress In Electromagnetics Research*, Vol. 130, 389–409, 2012.
 19. Pirhadi, A., M. Hakkak, and F. Keshmiri, "Using electromagnetic bandgap superstrate to enhance the bandwidth of probe-fed microstrip antenna," *Progress In Electromagnetic Research*, Vol. 61, 215–230, 2006.
 20. Liu, Y.-T., "Probe-fed patch antenna with an inclined patch for on-wall WLAN access point," *Progress In Electromagnetics Research Letters*, Vol. 18, 85–95, 2010.
 21. Huang, K.-C. and H.-F. Li, "A novel single-layer single-patch wide-band probe-feed crescentlike-shaped microstrip antenna," *Journal of Electromagnetic Waves and Applications*, Vol. 23, Nos. 2–3, 279–287, 2009.
 22. Deng, J.-Y., Y.-Z. Yin, L.-X. Guo, and F. Gao, "Double tuned patch antenna design for bandwidth enhancement," *2011 IEEE Int. Conf. Microwave Technology and Computational Electromagnetics*, 225–226, 2011.
 23. Kishk, A.-A., X. Zhang, A.-W. Glisson, and D. Kajfez, "Numerical analysis of stacked dielectric resonator antennas excited by a coaxial probe for wideband applications," *IEEE Trans. Antennas Propag.*, Vol. 51, No. 8, 1996–2006, Aug. 2003.
 24. Oh, J. and K. Sarabandi, "Low profile, miniaturized, inductively coupled capacitively loaded monopole antenna," *IEEE Trans. Antennas Propag.*, Vol. 60, No. 3, 1206–1213, Mar. 2012.
 25. Li, N., X. Li, and S. Quan, "An ANN-based small-signal equivalent circuit model for MOSFET device," *Progress In Electromagnetic Research*, Vol. 122, 47–60, 2012.